J|A|C|S ARTICLES

Published on Web 05/20/2010

Crystal and Magnetic Structures and Properties of $BiMnO_{3+\delta}$

Alexei A. Belik,*[,†] Katsuaki Kodama,[‡] Naoki Igawa,[‡] Shin-ichi Shamoto,[‡] Kosuke Kosuda,[§] and Eiji Takayama-Muromachi[†]

International Center for Materials Nanoarchitectonics (MANA) and Materials Analysis Station (MAS), National Institute for Materials Science (NIMS), 1-1 Namiki, Tsukuba, Ibaraki 305-0044, Japan, and Quantum Beam Science Directorate, Japan Atomic Energy Agency, Tokai, Ibaraki 319-1195, Japan

Received March 9, 2010; E-mail: Alexei.BELIK@nims.go.jp

Abstract: Crystal and magnetic structures of $BiMnO_{3+\delta}$ ($\delta = 0.03$, 0.08, and 0.14) have been determined by the Rietveld method from neutron diffraction data at 8−10 and 290 K. $BiMnO_{3.03}$ (= $Bi_{0.99}Mn_{0.99}O_3$) crystallizes in a monoclinic system (the refinement was performed in space group $C2/c$; $Z = 8$; $a = 9.5313(3)$ Å, $b = 5.57791(17)$ Å, $c = 9.7375(4)$ Å, $\beta = 108.951(2)°$ at 290 K). $BiMnO_{3.08}$ (= $Bi_{0.974}Mn_{0.974}O_3$) crystallizes in space group $P2_1/c$ ($Z = 8$; $a = 9.5565(4)$ Å, $b = 5.51823(16)$ Å, $c = 9.7051(4)$ Å, $\beta = 109.442(3)°$ at 290 K). It was found that Mn vacancies are localized mainly in one Mn site (among three sites) in $Bi_{0.974}Mn_{0.974}O_3$. Vacancy-ordering and charge-ordering scenarios are suggested as possible reasons for the crystal symmetry change compared with $Bi_{0.99}Mn_{0.99}O_3$. $BiMnO_{3.03}$ and $BiMnO_{3.08}$ are ferromagnetic below $T_C = 82$ and 68 K, respectively, with magnetic moments along the monoclinic b axes. Refined magnetic moments at 10 K are $2.88(2)\mu_B$ in $BiMnO_{3.03}$ and $2.33(2)\mu_B$ in $BiMnO_{3.08}$. $BiMnO_{3.14}$ (= $Bi_{0.955}Mn_{0.955}O_3$) crystallizes in an orthorhombic system (space group $Pnma$; $Z = 4$; $a = 5.5136(4)$ Å, $b = 7.8069(8)$ Å, and $c = 5.5454(5)$ Å at 290 K), and its structure is similar to that of $LaMnO_{3.11}$−$LaMnO_{3.15}$. No magnetic reflections were found in $BiMnO_{3.14}$ down to 8 K, in agreement with its spin-glass magnetic state. Magnetic and chemical properties of $BiMnO_{3+\delta}$ ($0.02 \leq \delta \leq 0.14$) have also been investigated and compared with those of $LaMnO_{3+\delta}$. Systematic changes of magnetic parameters in $BiMnO_{3+\delta}$ were found to depend on δ.

1. Introduction

Bismuth-containing perovskites have attracted much attention as multiferroic and lead-free ferroelectric materials.[1−9] Multiferroic materials have at least two of the following properties: (anti)ferroelectricity, (anti)ferromagnetism, and ferroelasticity.[10] $BiFeO_3$ is the most studied multiferroic material because its synthesis is rather simple at ambient pressure and its ferroelectric Curie temperature, $T_E = 1100$ K, and antiferromagnetic Néel temperature, $T_N = 640$ K, are both well above room temperature.[11] Despite hundreds of papers on $BiFeO_3$, there are still unresolved and puzzling problems.[11] Other $BiMO_3$ (M = transition metals) materials are less studied because they require high pressure for their synthesis in bulk form. However, many of them can be prepared in the thin-film form due to stabilization by substrates.[1] Among $BiMO_3$, $BiCoO_3$ also has a very large spontaneous polarization and $T_N = 470$ K above room temperature.[12]

$BiMnO_3$ is the only compound among $BiMO_3$ with a true ferromagnetic state below $T_C = 100$ K.[13,14] However, there is no consensus in the literature about its ferroelectric properties. Ideal $BiMnO_3$ should crystallize in centrosymmetric space group $C2/c$.[15] However, thin-film samples demonstrate ferroelectric hysteresis loops. First-principles calculations showed that the strain in thin films is not responsible for ferroelectric distortion.[16] Neutron powder diffraction data showed that the average structure of bulk $BiMnO_3$ is indeed very well described by the $C2/c$ model.[13,14] Single-crystal structural studies of $BiMnO_3$ also confirmed the $C2/c$ symmetry.[17] In terms of convergent-beam electron diffraction, the space group of bulk $BiMnO_3$ was

[†] MANA, NIMS.
[‡] Japan Atomic Energy Agency.
[§] MAS, NIMS.

(1) Ramesh, R.; Spaldin, N. A. *Nat. Mater.* **2007**, *6*, 21.
(2) Eerenstein, W.; Mathur, N. D.; Scott, J. F. *Nature* **2006**, *442*, 759.
(3) Khomskii, D. I. *J. Magn. Magn. Mater.* **2006**, *306*, 1.
(4) Fiebig, M. *J. Phys. D: Appl. Phys.* **2005**, *38*, R123.
(5) Baettig, P.; Ederer, C.; Spaldin, N. A. *Phys. Rev. B* **2005**, *72*, 214105.
(6) (a) Azuma, M.; Takata, K.; Saito, T.; Ishiwata, S.; Shimakawa, Y.; Takano, M. *J. Am. Chem. Soc.* **2005**, *127*, 8889. (b) Bridges, C. A.; Allix, M.; Suchomel, M. R.; Kuang, X. J.; Sterianou, I.; Sinclair, D. C.; Rosseinsky, M. J. *Angew. Chem., Int. Ed.* **2007**, *46*, 8787. (c) Claridge, J. B.; et al. *J. Am. Chem. Soc.* **2009**, *131*, 14000.
(7) Ishiwata, S.; Azuma, M.; Takano, M. *Chem. Mater.* **2007**, *19*, 1964.
(8) Zylberberg, J.; Belik, A. A.; Takayama-Muromachi, E.; Ye, Z. G. *Chem. Mater.* **2007**, *19*, 6385.
(9) Baettig, P.; Schelle, C. F.; LeSar, R.; Waghmare, U. V.; Spaldin, N. A. *Chem. Mater.* **2005**, *17*, 1376.
(10) Hill, N. A. *J. Phys. Chem. B* **2000**, *104*, 6694.
(11) Catalan, G.; Scott, J. F. *Adv. Mater.* **2009**, *21*, 2463.
(12) Belik, A. A.; Iikubo, S.; Kodama, K.; Igawa, N.; Shamoto, S.; Niitaka, S.; Azuma, M.; Shimakawa, Y.; Takano, M.; Izumi, F.; Takayama-Muromachi, E. *Chem. Mater.* **2006**, *18*, 798.
(13) Belik, A. A.; Iikubo, S.; Yokosawa, T.; Kodama, K.; Igawa, N.; Shamoto, S.; Azuma, M.; Takano, M.; Kimoto, K.; Matsui, Y.; Takayama-Muromachi, E. *J. Am. Chem. Soc.* **2007**, *129*, 971.
(14) Montanari, E.; Calestani, G.; Righi, L.; Gilioli, E.; Bolzoni, F.; Knight, K. S.; Radaelli, P. G. *Phys. Rev. B* **2007**, *75*, 220101(R).
(15) Baettig, P.; Seshadri, R.; Spaldin, N. A. *J. Am. Chem. Soc.* **2007**, *129*, 9854.
(16) Hatt, A. J.; Spaldin, N. A. *Eur. Phys. J. B* **2009**, *71*, 435.
(17) Toulemonde, P.; Darie, C.; Goujon, C.; Legendre, M.; Mendonca, T.; Alvarez-Murga, M.; Simonet, V.; Bordet, P.; Bouvier, P.; Kreisel, J.; Mezouar, M. *High Pressure Res.* **2009**, *29*, 600.

determined to be $C2/c$.[18] However, careful selected-area electron diffraction studies showed a long-range ordered structure with $C2$ symmetry and a short-range ordered structure with $P2$ or $P2_1$ symmetry.[18] The local symmetry of bulk $BiMnO_3$ was suggested to be $P2$ or $P2_1$ by atomic pair distribution function analysis.[19] It is possible that the oxygen content plays a crucial role.

Despite the many reports on $BiMnO_3$, the effects of oxygen stoichiometry were investigated only in refs 20 and 21. On the other hand, the effects of the oxygen content on the structure and properties of $LaMnO_{3+\delta}$ have been more extensively investigated,[22−25] with numerous controversial reports in the past. Today, the following changes are established: the low-temperature magnetic phase of $LaMnO_{3+\delta}$ changes from insulating antiferromagnetic to insulating ferromagnetic at small δ, keeping similar orthorhombic structure ($a = 5.4954$ Å, $b = 7.7854$ Å, and $c = 5.5355$ Å in *Pnma*), almost identical Mn−O distances (1.98 Å × 6), and inverse a and c parameters.[22] Stoichiometric $LaMnO_3$ has $a = 5.7385$ Å, $b = 7.7024$ Å, and $c = 5.5378$ Å and two long Mn−O distances (2.18 Å × 2, 1.91 Å × 2, and 1.97 Å × 2) due to the Jahn−Teller effect.[22] There is a change in symmetry from orthorhombic to rhombohedral at larger δ in $LaMnO_{3+\delta}$ and a change from insulating ferromagnetic to metallic ferromagnetic states.[22−25] Note that even though the formula is written as $LaMnO_{3+\delta}$ for simplicity, cation vacancies $La_{1-x}Mn_{1-x}O_3$ are actually formed in perovskite structures. In $BiMnO_{3\pm\delta}$, Sundaresan et al.[20] also found symmetry and property changes depending on δ. However, they reported oxygen deficiency from $BiMnO_{2.84}$ to $BiMnO_{2.99}$ in comparison with the $LaMnO_{3+\delta}$ system. In ref 21, symmetry changes from $C2/c$ (phase I) to $C2/c$ (phase II) to $P2_1/c$ (P-phase) to *Pnma* (O-phase) have been established on the basis of X-ray powder diffraction (XRD) data of oxygen hyperstoichiometric $BiMnO_{3+\delta}$. Crystal and magnetic structures of $BiMnO_{3+\delta}$ have not been determined yet.

In this work, we determine for the first time the crystal and magnetic structures of $BiMnO_{3+\delta}$ ($\delta = 0.03$, 0.08, and 0.14) by the Rietveld method from neutron powder diffraction data measured at 8−10 and 290 K. Neutron diffraction confirmed the onset of long-range ferromagnetic order in $BiMnO_{3.03}$ and $BiMnO_{3.08}$ and the suggested[21] spin-glass state in $BiMnO_{3.14}$. Magnetic and chemical properties of $BiMnO_{3+\delta}$ ($0.02 \le \delta \le 0.14$) have also been investigated, and systematic changes of magnetic parameters were found as a function of δ.

2. Experimental Section

2.1. Synthesis. $BiMnO_{3+\delta}$ ($0.02 \le \delta \le 0.16$) samples were prepared from stoichiometric mixtures of Bi_2O_3 (99.9999%, Rare Metallic Co. Ltd.), MnO_2 (99.997%, Alfa Aesar), and Mn_2O_3. The phase purity and oxygen content of MnO_2 were confirmed by XRD and thermogravimetric analysis (TGA). MnO_2 was the well-crystallized single-phase α modification. MnO_2 was heated in air to 923 K in 5 h and soaked there for 24 h (the experiment was performed in a conventional muffle furnace; the sample weights were measured before and after annealing). The final product was well-crystallized single-phase Mn_2O_3 (Mn_2O_3 obtained in this way was used as the starting chemical). The oxygen content of the original raw material, calculated from the weight loss, corresponded to $MnO_{2.01}$. The synthesis of $BiMnO_{3+\delta}$ was performed in a belt-type high-pressure apparatus at 6 GPa and 1600 K for 40 min in sealed Pt capsules. After heat treatment, the samples were quenched to room temperature, and the pressure was slowly released. The resultant samples were black loose ($0.0 \le \delta \le 0.04$) or dense ($0.06 \le \delta \le 0.16$) pellets.

2.2. Neutron Powder Diffraction Experiments and Structure Refinements. Neutron powder diffraction data of $BiMnO_{3+\delta}$ ($\delta = 0.03$, 0.08, and 0.14) were collected at 8−10 and 290 K with the high-resolution powder diffractometer installed at the JRR-3 reactor at the Japan Atomic Energy Agency (JAEA, Tokai, Japan). The incident neutron wavelength was 1.8233(10) Å. About 5 g of each sample was contained in a V holder (diameter: 6.0 mm) filled with He. A cryostat containing the holder was slowly oscillated during the measurement. The data were taken with a step of ca. 0.05° in a 2θ range between 2.5 and 162° with 64 ^{3}He detectors.

The neutron powder diffraction data were analyzed by the Rietveld method with RIETAN-2000.[26] The background was represented by an eighth-order Legendre polynomial. The pseudo-Voigt function of Toraya[27] was used as a profile function. Isotropic atomic displacement parameters, B, with the isotropic Debye−Waller factor represented as $\exp(-B \sin^2\theta/\lambda^2)$, were assigned to all the sites. Bound coherent scattering lengths, b_c, used for the structure refinements were 8.532 (Bi), −3.750 (Mn), and 5.803 fm (O).[28] Coefficients for analytical approximations to the magnetic form factor of Mn^{3+} were taken from ref 29.

2.3. Physical and Chemical Properties. Magnetic properties were measured on a SQUID magnetometer (Quantum Design, MPMS) between 2 and 400 K in applied fields of 100 Oe, 1 kOe, and 10 kOe under both zero-field-cooled (ZFC) and field-cooled (FC; on cooling) conditions. Isothermal magnetization measurements were performed between −50 and 50 kOe at 5 K. Specific heat, C_p, at magnetic fields of 0 and 70 kOe was recorded between 2 and 300 K on cooling by a pulse relaxation method using a commercial calorimeter (Quantum Design PPMS).

TGA curves of some selected $BiMnO_{3+\delta}$ samples were recorded in high-purity Ar on a Perkin-Elmer Pyris 1 TGA system between 293 and 773 K at a heating rate of 10 K/min in an Al_2O_3 holder. Differential scanning calorimetry (DSC) curves were recorded on a Mettler Toledo DSC1 STAR^e system at a heating/cooling rate of 20 K/min under N_2 flow from 293 to 673 K in Al capsules (two runs).

The cation ratio of some selected samples and $BiMnO_3$ was determined by electron probe microanalysis (EPMA) using a JEOL JXA-8500F instrument. The surface was polished on a fine alumina (1 μm)-coated film before the EPMA measurements. MnO and $Bi_4Ge_3O_{12}$ were used as standard materials for Mn and Bi. The Mn:Bi ratio determined by EPMA was 1.05(6) in $BiMnO_3$, 1.005(15) in $BiMnO_{3.08}$, and 1.011(16) in $BiMnO_{3.14}$. A larger error in $BiMnO_3$ is probably related to the quality of the surface because the pellet of $BiMnO_3$ was very loose compared with dense pellets of $BiMnO_{3.08}$ and $BiMnO_{3.14}$.

(18) Yokosawa, T.; Belik, A. A.; Asaka, T.; Kimoto, K.; Takayama-Muromachi, E.; Matsui, Y. *Phys. Rev. B* **2008**, *77*, 024111.
(19) Kodama, K.; Iikubo, S.; Shamoto, S.; Belik, A. A.; Takayama-Muromachi, E. *J. Phys. Soc. Jpn.* **2007**, *76*, 124605.
(20) Sundaresan, A.; Mangalam, R. V. K.; Iyo, A.; Tanaka, Y.; Rao, C. N. R. *J. Mater. Chem.* **2008**, *18*, 2191.
(21) Belik, A. A.; Kolodiazhnyi, T.; Kosuda, K.; Takayama-Muromachi, E. *J. Mater. Chem.* **2009**, *19*, 1593.
(22) Huang, Q.; Santoro, A.; Lynn, J. W.; Erwin, R. W.; Borchers, J. A.; Peng, J. L.; Greene, R. L. *Phys. Rev. B* **1997**, *55*, 14987.
(23) Alonso, J. A.; Martinez-Lope, M. J.; Casais, M. T.; MacManus-Driscoll, J. L.; de Silva, P. S. I. P. N.; Cohen, L. F.; Fernandez-Diaz, M. T. *J. Mater. Chem.* **1997**, *7*, 2139.
(24) Topfer, J.; Goodenough, J. B. *J. Solid State Chem.* **1997**, *130*, 117.
(25) Maurin, I.; Barboux, P.; Lassailly, Y.; Boilot, J. P.; Villain, F.; Dordor, P. *J. Solid State Chem.* **2001**, *160*, 123.
(26) Izumi, F.; Ikeda, T. *Mater. Sci. Forum* **2000**, *321−324*, 198.
(27) Toraya, H. *J. Appl. Crystallogr.* **1990**, *23*, 485.
(28) Sears, V. F. *International Tables for Crystallography*, 3rd ed.; Kluwer: Dordrecht, 2004; Vol. C, pp 445−452.
(29) Brown, P. J. *International Tables for Crystallography*, 3rd ed.; Kluwer: Dordrecht, 2004; Vol. C, p 454.

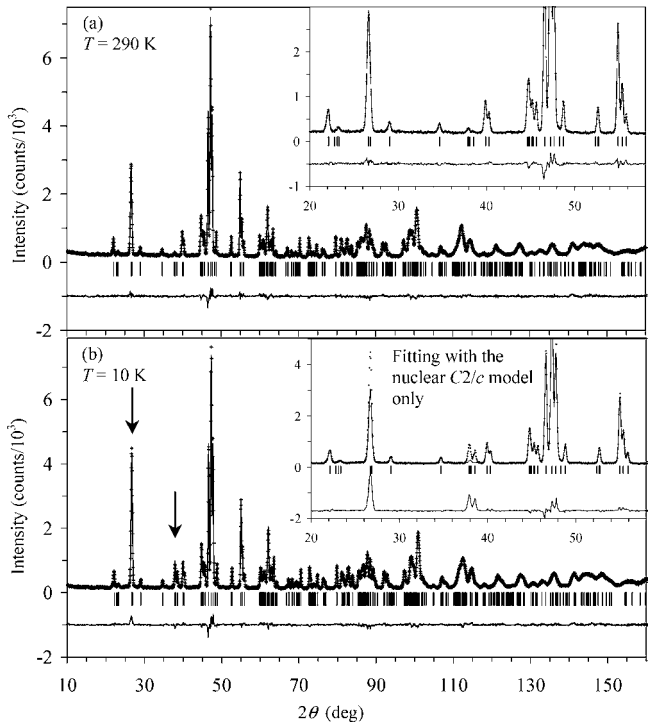

Figure 1. Observed (crosses), calculated (solid line), and difference neutron powder diffraction patterns for monoclinic $BiMnO_{3.03}$ (phase II) at (a) 290 K (the nuclear model) and (b) 10 K (the nuclear and magnetic models). Bragg reflections are indicated by tic marks. Inset in (a) shows the enlarged fragment of the fitting. Inset in (b) shows a fragment of the fitting results using only the nuclear model to emphasize magnetic reflections. Arrows show the magnetic reflections.

XRD data were collected at room temperature on a Rigaku Ultima III diffractometer using Cu K_α radiation (2θ range of 4−100°, a step width of 0.02°, and a counting time of 2−10 s/step).

3. Results

3.1. Structural Analysis of $BiMnO_{3.03}$. All the observed reflections on neutron diffraction patterns of $BiMnO_{3.03}$ at 290 K (and 10 K) could be indexed in a monoclinic system with $a \approx 9.53$ Å, $b \approx 5.58$ Å, $c \approx 9.74$ Å, and $\beta \approx 108.95°$. Reflection conditions derived from the indexed reflections were $h + k = 2n$ for hkl, and $h = 2n$ and $l = 2n$ for $h0l$, affording possible space groups Cc (No. 9) and $C2/c$ (No. 15).[30] Similar to $BiMnO_3$,[13] we used the maximum space group in Rietveld analysis of $BiMnO_{3.03}$ because this model gave very nice agreement between the observed and calculated patterns ($R_{wp} = 5.41\%$, $R_p = 4.28\%$, $R_B = 2.04\%$) and the most reliable bond lengths. We note that attempts to refine the structure in space group $C2$ ($R_{wp} = 5.18\%$, $R_p = 4.08\%$, $R_B = 1.78\%$) or Cc ($R_{wp} = 5.22\%$, $R_p = 4.13\%$, $R_B = 1.78\%$) did not visibly improve the fit. For starting fractional coordinates in the Rietveld analysis of $BiMnO_{3.03}$, we used those of $BiMnO_3$ at 550 K.[13] Because the deviation from the stoichiometry in $BiMnO_{3.03}$ ($= Bi_{0.99}Mn_{0.99}O_3$) is very small, we assumed random distribution of cation vacancies at the Bi and Mn sites, with $g(\mathrm{Bi}) = g(\mathrm{Mn1}) = g(\mathrm{Mn2}) = 0.99$, where g is the occupation factor.

At 10 K, no new reflections appeared, but a few reflections significantly changed their intensities and could not be fit with the nuclear model (Figure 1b, inset). They corresponded to magnetic scattering due to ferromagnetic order. The magnetic reflections could be indexed with the same lattice parameters as the chemical cell. Therefore, the three-dimensional long-range-ordered magnetic structure can be described in terms of a propagation vector $\boldsymbol{k} = (0,0,0)$, and we determined the crystal structure and magnetic moments assuming one phase with space group $C2/c$. Magnetic moments of Mn^{3+} were found to align along the monoclinic b axis, similar to the direction of magnetic moments of Mn^{3+} in $BiMnO_3$.[14] The following linear constraint was imposed on magnetic moments, μ, of the Mn sites: $\mu(\mathrm{Mn1}) = \mu(\mathrm{Mn2})$. Table 1 gives fractional coordinates, B parameters, lattice parameters, and R values resulting from the Rietveld refinement. Bond lengths, bond valence sums (BVS),[31] and distortion parameters of MnO_6, Δ, are given in the Supporting Information. Figure 1 displays observed, calculated, and difference neutron diffraction patterns at 10 and 290 K.

Table 1. Structure Parameters of $BiMnO_{3.03}$ at 10 and 290 K[a]

site	Wyckoff position	x	y	z	B (Å²)
Bi	8*f*	0.13395(13)	0.2145(2)	0.12874(18)	0.50(3)
		0.13347(14)	0.2155(2)	0.12775(20)	1.03(3)
Mn1	4*e*	0	0.2242(7)	0.75	0.34(10)
		0	0.2264(7)	0.75	0.11(10)
Mn2	4*d*	0.25	0.25	0.5	0.05(9)
		0.25	0.25	0.5	0.32(10)
O1	8*f*	0.0895(2)	0.1810(4)	0.5868(2)	0.88(4)
		0.0898(2)	0.1837(4)	0.5874(2)	1.15(4)
O2	8*f*	0.1536(2)	0.5549(3)	0.3706(3)	1.10(4)
		0.1539(2)	0.5549(4)	0.3708(3)	1.68(5)
O3	8*f*	0.3541(2)	0.5462(3)	0.1600(2)	0.91(4)
		0.3543(2)	0.5472(4)	0.1593(2)	1.42(5)

[a] Space group $C2/c$ (No. 15); $Z = 8$. The first (x, y, z, and B) line of each site is for 10 K, and the second one is for 290 K. $g(\mathrm{Bi}) = g(\mathrm{Mn1}) = g(\mathrm{Mn2}) = 0.99$ and $g(\mathrm{O1}) = g(\mathrm{O2}) = g(\mathrm{O3}) = 1$, where g is the occupation factor. At 10 K, $a = 9.5166(3)$ Å, $b = 5.56813(15)$ Å, $c = 9.7369(3)$ Å, $\beta = 109.029(2)°$, and $V = 487.76(3)$ Å³, $R_{wp} = 5.87\%$ ($S = R_{wp}/R_e = 1.16$), $R_p = 4.61\%$, $R_B = 2.20\%$, and $R_F = 1.07\%$, $\mu = 2.88(2)\ \mu_B$. At 290 K, $a = 9.5313(3)$ Å, $b = 5.57791(17)$ Å, $c = 9.7375(4)$ Å, $\beta = 108.951(2)°$, and $V = 489.63(3)$ Å³, $R_{wp} = 5.41\%$ ($S = 1.06$), $R_p = 4.28\%$, $R_B = 2.04\%$, and $R_F = 1.04\%$.

Even though the R values are smaller for the $C2$ and Cc models (as expected because of the almost doubled number of refined structural parameters), the standard deviations of fractional coordinates are about 1 order of magnitude larger than those of the $C2/c$ model (see the Supporting Information for structural data in the $C2$ and Cc models). This fact shows the existence of strong correlations in the structural parameters for the non-centrosymmetric models. In addition, some B parameters were negative in the $C2$ model, and the $C2$ model gives unreasonable BVS values of +3.40 for Mn1a and +2.54 for Mn1b. Unreasonable BVS values of some Mn sites were observed in stoichiometric $BiMnO_3$ when the refinement was performed in the $C2$ model.[13] Model-independent Le Bail fits in the $C2/c$ model resulted in $R_{wp} = 4.52\%$ and $R_p = 3.50\%$.

3.2. Structural Analysis of $BiMnO_{3.08}$. All the observed reflections of $BiMnO_{3.08}$ at 290 K (and 10 K) could be indexed in a monoclinic system with $a \approx 9.56$ Å, $b \approx 5.52$ Å, $c \approx 9.71$ Å, and $\beta \approx 109.44°$. Reflection conditions derived from the indexed reflections were $l = 2n$ for $h0l$, $h00$, and $00l$ and $k = 2n$ for $0k0$, affording one possible space group, $P2_1/c$ (No. 14).[30] We emphasize that it is the maximum possible space group because some observed reflection conditions may be broken if the corresponding reflections are very weak or overlap with other reflections. However, the fitting results were very good in the

(30) *International Tables for Crystallography*, 5th ed.; Hahn, T., Ed.; Kluwer: Dordrecht, 2002; Vol. A, p 52.

(31) Brese, R. E.; O'Keeffe, M. *Acta Crystallogr., Sect. B* **1991**, *47*, 192.

Table 2. Structure Parameters of $BiMnO_{3.08}$ at 10 and 290 K[a]

site	Wyckoff position	*x*	*y*	*z*	*B* (Å^2)
Bi1	4*e*	0.3801(5)	0.4835(6)	0.1357(5)	1.91(8)
		0.3789(5)	0.4842(7)	0.1357(5)	2.36(8)
Bi2	4*e*	0.1168(4)	0.4632(6)	0.3746(4)	0.79(6)
		0.1171(5)	0.4670(7)	0.3753(4)	1.46(7)
Mn1	4*e*	0.2474(10)	0.0200(8)	0.2401(7)	0.20(12)
		0.2505(10)	0.0215(9)	0.2418(8)	0.63(13)
Mn2	2*b*	0.5	0	0	0.19(19)
		0.5	0	0	0.48(21)
Mn3	2*c*	0.0	0.0	0.5	0.19(19)
		0.0	0.0	0.5	0.22(20)
O1	4*e*	0.3344(5)	0.4424(9)	0.5726(5)	0.41(10)
		0.3360(5)	0.4439(9)	0.5737(5)	0.50(10)
O2	4*e*	0.1497(6)	0.4431(12)	0.8918(5)	1.70(11)
		0.1492(7)	0.4448(13)	0.8909(5)	2.29(12)
O3	4*e*	0.3922(5)	0.7818(10)	0.3422(5)	1.53(11)
		0.3909(6)	0.7783(10)	0.3412(6)	2.06(11)
O4	4*e*	0.0970(6)	0.8069(9)	0.1078(5)	1.21(10)
		0.0964(6)	0.8063(11)	0.1076(6)	1.87(11)
O5	4*e*	0.5858(5)	0.7714(11)	0.1591(5)	1.23(10)
		0.5856(5)	0.7714(11)	0.1579(5)	1.52(11)
O6	4*e*	0.8706(6)	0.8086(9)	0.3434(5)	1.20(10)
		0.8705(6)	0.8083(9)	0.3438(5)	1.49(10)

[a] Space group $P2_1/c$ (No. 14); $Z = 8$. The first (*x*, *y*, *z*, and *B*) line of each site is for 10 K, and the second one is for 290 K. g(Bi1) = g(Bi2) = 0.974, g(Mn1) = 0.948, and g(Mn2) = g(Mn3) = g(O1) = g(O2) = g(O3) = g(O4) = g(O5) = g(O6) = 1, where g is the occupation factor. At 10 K, a = 9.5387(4) Å, b = 5.51159(15) Å, c = 9.6967(3) Å, β = 109.433(2)°, and V = 480.75(3) Å^3, R_{wp} = 5.70% (S = 1.42), R_p = 4.15%, R_B = 2.31%, and R_F = 1.04%, μ = 2.33(2)μ_B. At 290 K, a = 9.5565(4) Å, b = 5.51823(16) Å, c = 9.7051(4) Å, β = 109.442(3)°, and V = 482.61(3) Å^3, R_{wp} = 5.21% (S = 1.29), R_p = 3.89%, R_B = 2.54%, and R_F = 1.37%.

$P2_1/c$ model (R_{wp} = 5.21%, R_p = 3.89%, R_B = 2.54%). The $P2_1/c$ model already has a lot of refined structural parameters, and attempts to reduce the symmetry to non-centrosymmetric models resulted in unreasonable structural (thermal) parameters and bond lengths. Model-independent Le Bail fits in the $P2_1/c$ model resulted in R_{wp} = 4.13% and R_p = 2.74%. For starting fractional coordinates in the Rietveld analysis of $BiMnO_{3.08}$, we used those of $BiMnO_{3.03}$ at 290 K, transformed from space group $C2/c$ to $P2_1/c$ (note that $P2_1/c$ is a subgroup of $C2/c$).

The $P2_1/c$ model has three Mn sites. The refinement of their occupancies resulted in g(Mn1) = 0.924(14), g(Mn2) = 1.01(2), and g(Mn3) = 0.98(3), with fixed B(Mn1) = B(Mn2) = B(Mn3) = 0.5 Å^2. These results suggested that the Mn vacancies in $BiMnO_{3.08}$ (= $Bi_{0.974}Mn_{0.974}O_3$) are mainly localized at the Mn1 site. Therefore, in the final stage, we fixed the g values as g(Mn1) = 0.948 and g(Mn2) = g(Mn3) = 1. In addition, no anomalies were found at the Bi sites. Therefore, we assumed random distribution of the Bi vacancies with g(Bi1) = g(Bi2) = 0.974.

At 10 K, no new reflections appeared, but a few reflections significantly changed their intensities, similar to the observation for $BiMnO_{3.03}$. Therefore, we assumed the same magnetic structure with magnetic moments of Mn^{3+} aligned along the monoclinic *b* axis. The following linear constraint was imposed on magnetic moments, μ, of the Mn sites: μ(Mn1) = μ(Mn2) = μ(Mn3). Table 2 gives fractional coordinates, *B* parameters, lattice parameters, and *R* values resulting from the Rietveld refinement. Bond lengths and BVS and Δ values are given in the Supporting Information. Figure 2 displays observed, calculated, and difference neutron diffraction patterns at 10 and 290 K. Figure 3 shows the fragments of the crystal structures of $BiMnO_{3.03}$ and $BiMnO_{3.08}$.

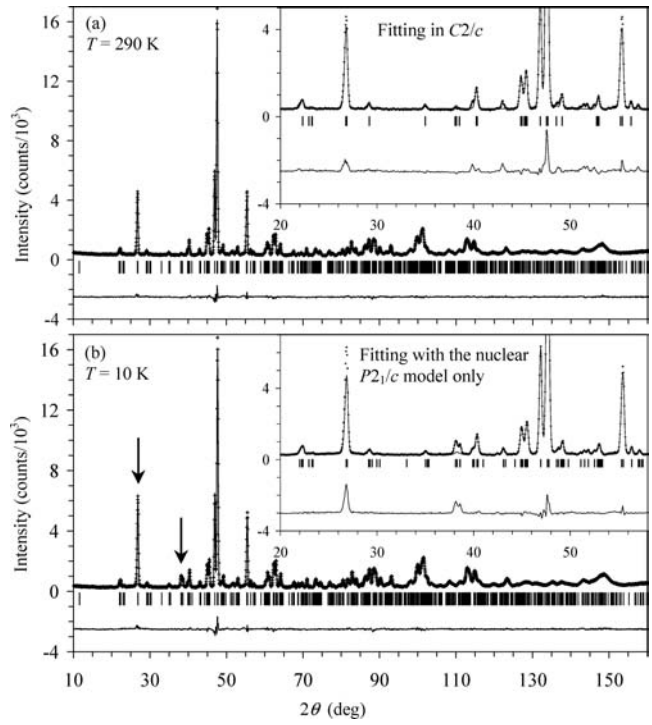

Figure 2. Observed (crosses), calculated (solid line), and difference neutron powder diffraction patterns for monoclinic $BiMnO_{3.08}$ (P-phase) at (a) 290 K (the nuclear model) and (b) 10 K (the nuclear and magnetic models). Bragg reflections are indicated by tic marks. Inset in (a) shows a fragment of the fitting results in the $C2/c$ model to emphasize additional reflections of the $P2_1/c$ model. Inset in (b) shows a fragment of the fitting results using only the nuclear $P2_1/c$ model to emphasize magnetic reflections. Arrows show the magnetic reflections.

3.3. Structural Analysis of $BiMnO_{3.14}$. The sample prepared in a large amount for neutron diffraction contained weak reflections from unidentified impurities. All main reflections observed on the neutron patterns of $BiMnO_{3.14}$ at 290 K (and 8 K) could be indexed in an orthorhombic system with $a \approx 5.51$ Å, $b \approx 7.81$ Å, $c \approx 5.55$ Å. For starting fractional coordinates in Rietveld analysis of $BiMnO_{3.14}$ (= $Bi_{0.955}Mn_{0.955}O_3$) we used those of $LaMnO_{3+\delta}$ ($LaMnO_3$-IIb) in space group *Pnma*.[22] No additional reflections or changes in intensities of the nuclear reflections were observed at 8 K. This result shows that there is no long-range magnetic ordering in $BiMnO_{3.14}$. Fractional coordinates, *B* parameters, lattice parameters, *R* values, bond lengths, and BVS and Δ values are given in the Supporting Information. Figure 4 displays observed, calculated, and difference neutron diffraction patterns at 8 and 290 K.

3.4. X-ray Powder Diffraction of $BiMnO_{3+\delta}$ ($0.0 \le \delta \le 0.16$). Figure 5 depicts XRD patterns of $BiMnO_{3+\delta}$ ($0.0 \le \delta \le 0.16$). $BiMnO_3$ crystallizes in the monoclinic phase I structure[13] in space group $C2/c$. $BiMnO_{3+\delta}$ ($0.02 \le \delta \le 0.04$) has the monoclinic phase II structure[13] with space group $C2/c$. The lattice parameter c and the monoclinic angle β drop noticeably during the structural change from phase I to phase II (Figure 6). $BiMnO_{3+\delta}$ ($0.06 \le \delta \le 0.08$) has the monoclinic P-phase[32] structure with space group $P2_1/c$. The lattice parameter b drops and the monoclinic angle β and the lattice parameter a jump noticeably during the structural change from phase II to P-phase. Similar changes of the lattice parameters were found in stoichiometric $BiMnO_3$ during the transition from phase I to

(32) Belik, A. A.; Yusa, H.; Hirao, N.; Ohishi, Y.; Takayama-Muromachi, E. *Inorg. Chem.* **2009**, *48*, 1000.

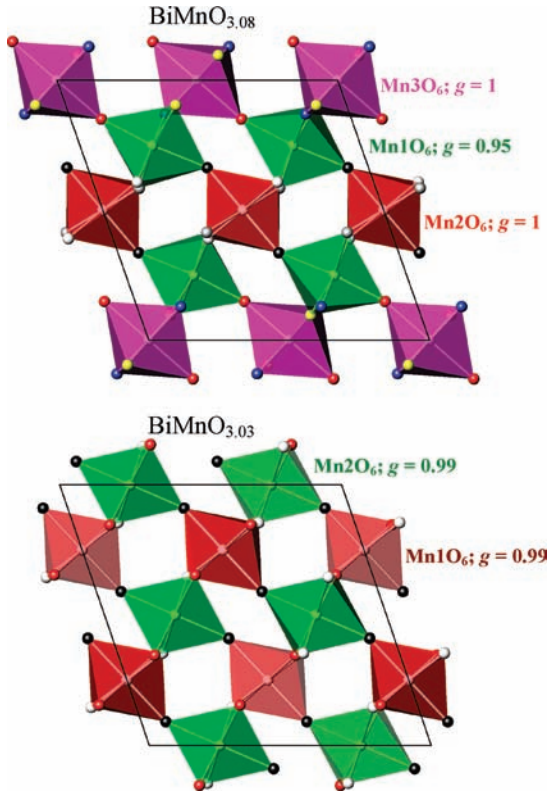

Figure 3. Fragments of the crystal structures of $BiMnO_{3.08}$ (top) and $BiMnO_{3.03}$ (bottom) viewed along the monoclinic *b* axis. Only the MnO_6 octahedra are shown. *g* is the occupation factor of each site.

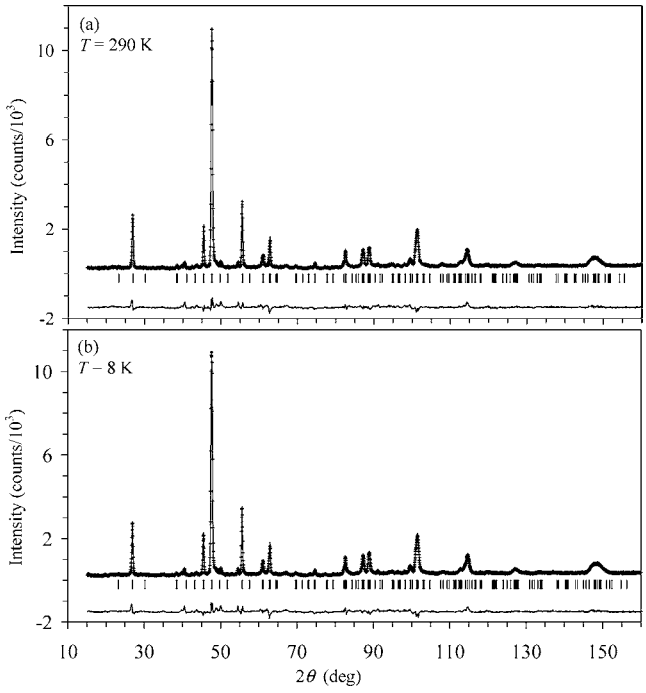

Figure 4. Observed (crosses), calculated (solid line), and difference neutron powder diffraction patterns for orthorhombic $BiMnO_{3.14}$ at (a) 290 K and (b) 8 K. Bragg reflections are indicated by tic marks.

P-phase at high pressure.[32] Therefore, phases I and II and P-phase can be distinguished by their lattice parameters. $BiMnO_{3+\delta}$ ($0.10 \le \delta \le 0.12$) samples were mixtures of the P-phase and orthorhombic O-phase. $BiMnO_{3.14}$ (prepared in a small amount) had one orthorhombic O-phase (see the Supporting Information), and $BiMnO_{3.16}$ contained an impurity with the $Bi_3Mn_3O_{11}$-type structure.[33]

3.5. Magnetic Properties of $BiMnO_{3+\delta}$. Figure 7 shows the χ vs *T* curves of $BiMnO_{3+\delta}$ ($0.02 \le \delta \le 0.14$) measured at 100 Oe. Figure 8 gives the inverse FC magnetic susceptibilities measured at 10 kOe. Surprisingly, four δ regions can be seen from this plot, corresponding to the samples with different symmetries (II, P, and O) and different phase compositions (P+O). Figure 9 depicts the isothermal magnetization curves at 5 K. The saturation magnetization at 50 kOe is strongly dependent on the symmetry [monoclinic (II and P) or orthorhombic (O)] and magnetic properties (ferromagnetic or spin-glass). As a result, the two-phase samples with $\delta = 0.10$ and 0.12 can clearly be seen from these measurements. Magnetic parameters are summarized in Table 3.

Specific heat data are given in the Supporting Information. $BiMnO_{3+\delta}$ ($0.0 \le \delta \le 0.08$) showed anomalies near T_C at zero magnetic field, confirming long-range magnetic ordering. A magnetic field of 70 kOe smeared the anomalies and moved the magnetic part of specific heat to a high-temperature region, which is typical for ferromagnets. $BiMnO_{3.14}$, for which a spin-glass transition was suggested[21] and no magnetic reflections were observed on the neutron diffraction pattern at 8 K, showed no anomalies on specific heat.

3.6. Thermal Properties of $BiMnO_{3+\delta}$. The first heating DSC curve of $BiMnO_{3.03}$ showed no anomalies. However, an anomaly was observed on the first (and second) cooling curve near 410 K and on the second heating curve at 440 K (see the Supporting Information). The XRD pattern [collected after the DSC experiments up to 673 K (two runs)] showed that $BiMnO_{3.03}$ with the phase II structure transformed to a new phase with the phase I structure (see the Supporting Information). The TGA analysis showed that this transformation starts around 420 K. The stoichiometric $BiMnO_3$ has the phase transition at $T_{OO} = 474$ K.[13] Therefore, the difference in the phase transition temperatures (440 vs 474 K) is due to the slightly different oxygen content.

$BiMnO_{3.06}$ showed DSC anomalies near 540 K on heating (two runs) and near 500 K on cooling (two runs). The temperature stability of the anomalies indicates that the phase transition is intrinsic, and there are no significant changes in the oxygen content. Nevertheless, very small changes in the XRD patterns of the as-prepared $BiMnO_{3.06}$ and after the DSC experiment up to 673 K (two runs) could be detected (see the Supporting Information).

$BiMnO_{3.14}$ had no DSC anomalies up to 673 K, and no changes in the XRD patterns were found before and after heating.

4. Discussion

Using the high-pressure technique, we could prepare high-quality $BiMnO_{3+\delta}$ samples. The high-pressure synthesis has significant advantages in controlling the oxygen content. Under certain conditions (listed below), the final chemical composition of products is the same as the target composition. The necessary conditions are (1) absence of a reaction between a capsule and a product, (2) absence of weight change of a capsule (with a sample inside) and absence of gas release when a capsule is opened, and (3) absence of secondary phases (if secondary phases are present, the overall chemical composition of a phase

(33) Belik, A. A.; Takayama-Muromachi, E. *J. Am. Chem. Soc.* **2009**, *131*, 9504.

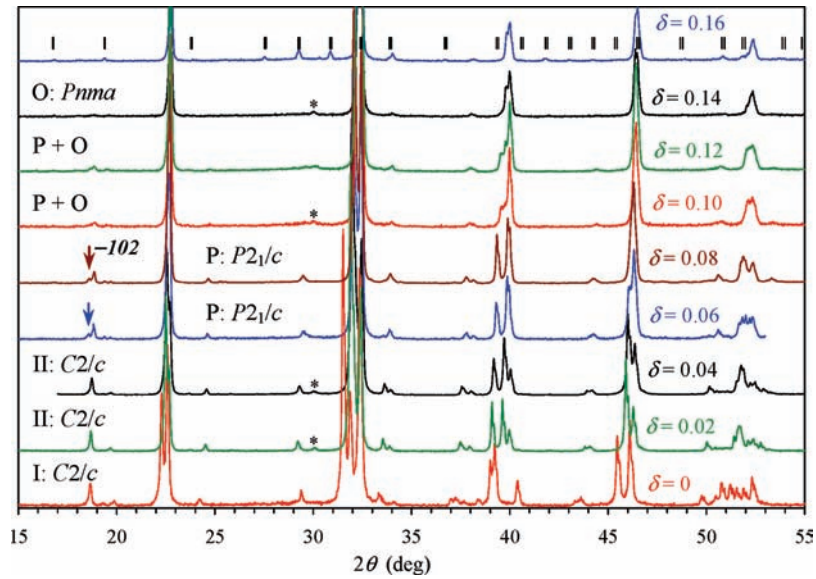

Figure 5. X-ray powder diffraction patterns of $BiMnO_{3+\delta}$ ($0.0 \le \delta \le 0.16$) measured with Cu Kα radiation at room temperature. I, composition with the phase I structure; II, composition with the phase II structure; P, composition with the P-phase structure; O, composition with the orthorhombic O structure. Arrows depict the characteristic additional reflection of the P-phase. Tic marks show the position of Bragg reflections for the $Bi_3Mn_3O_{11}$-type impurity phase in $BiMnO_{3.16}$. Asterisks show the strongest reflection of $Bi_2O_2CO_3$; this phase sometimes appears in a trace amount.

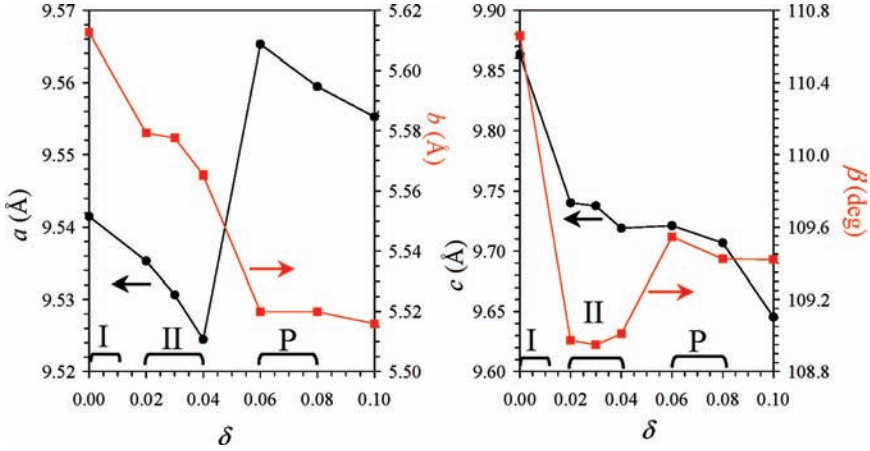

Figure 6. Lattice parameters of monoclinic phases (phase I, phase II, and P-phase) in $BiMnO_{3+\delta}$ ($0.0 \le \delta \le 0.10$) as a function of the oxygen content δ. $BiMnO_{3.10}$ was a mixture of P-phase and O-phase; nevertheless, the lattice parameters of the P-phase could be refined.

mixture will be the same as the target composition). All these conditions have been fulfilled during the synthesis of $BiMnO_{3+\delta}$. The oxygen content of the final products was also confirmed by TGA in a mixture of 3% H_2 + 97% Ar using a Perkin-Elmer Pyris 1 TGA system in Al_2O_3 holders (samples were heated to 870 K at a heating rate of 5 K/min and soaked there for 1 h). The calculated oxygen content was the same as the target one within $\delta \pm 0.01$ (see the Supporting Information). The preparation of Bi-containing perovskites ($BiMO_3$) of high quality is rather difficult. Even $BiFeO_3$ is quite hard to make single-phase.[34] $BiMnO_{3+\delta}$ cannot be prepared at ambient pressure at all. However, solid solutions of $BiFeO_3-BiMnO_3$ in the $BiFeO_3$-rich site can easily be prepared at ambient pressure with good quality.[35] Because the synthesis takes place in an open environment, the oxygen content is changing, and oxygen hyperstoichiometric samples $BiFe_{1-x}Mn_xO_{3+\delta}$ are formed.

$BiMnO_{3.03}$ and $BiMnO_3$ crystallize in the same space group. The analysis of the Mn−O bond lengths suggests that $BiMnO_{3.03}$ is very close to the phase II modification of $BiMnO_3$ at 550 K (see the Supporting Information)[13] or to $BiMn_{1-x}M_xO_3$ at room temperature.[36,37] It is believed that orbital order disappears in $BiMnO_3$ above $T_{OO} = 470$ K. Therefore, our structural results show that introduction of a small amount of Mn^{4+} ions ($Bi_{0.99}Mn^{3+}_{0.931}Mn^{4+}_{0.059}O_3$) destroys the orbital ordered state in $BiMnO_{3.03}$. This effect is similar to the effect of isovalent substitution in the Mn sublattice, where the orbital ordered phase disappeared near $x = 0.05$ in $BiMn_{1-x}Sc_xO_3$.[36]

Because the crystal structures of $BiMnO_{3.03}$ and $BiMnO_3$ are very similar to each other, $BiMnO_{3.03}$ easily transforms to $BiMnO_{3+\delta}$ ($\delta \approx 0$) on heating in an inert atmosphere, starting just from 420 K. We also found that the stoichiometric bulk $BiMnO_3$ transforms to an oxygen-deficient modification having

(34) Valant, M.; Axelsson, A. K.; Alford, N. *Chem. Mater.* **2007**, *19*, 5431.
(35) Selbach, S. M.; Tybell, T.; Einarsrud, M. A.; Grande, T. *Chem. Mater.* **2009**, *21*, 5176.
(36) Belik, A. A.; Kato, K.; Takayama-Muromachi, E. *J. Solid State Chem.* **2009**, *182*, 685.
(37) Belik, A. A.; Takayama-Muromachi, E. *Mater. Res. Bull.* **2008**, *43*, 3179.

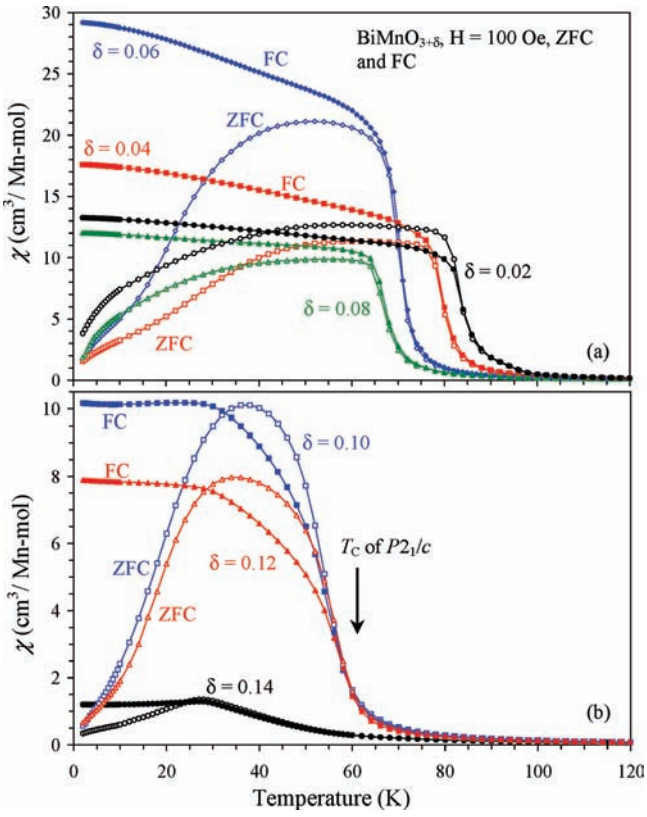

Figure 7. ZFC (open symbols) and FC (filled symbols) dc magnetic susceptibility ($\chi = \mathbf{M}/\mathbf{H}$) curves measured at 100 Oe for (a) $BiMnO_{3+\delta}$ with $\delta = 0.02$, 0.04, 0.06, and 0.08 and (b) the two-phase $BiMnO_{3+\delta}$ samples with $\delta = 0.10$ and 0.12 and orthorhombic $BiMnO_{3.14}$.

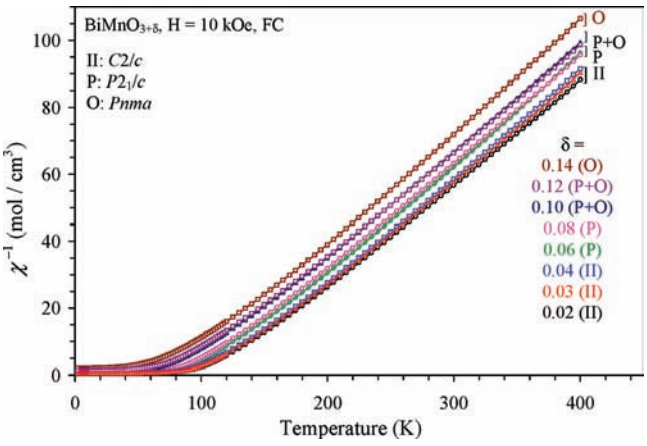

Figure 8. Inverse magnetic susceptibilities of $BiMnO_{3+\delta}$ ($0.02 \le \delta \le 0.14$) measured at 10 kOe in the FC mode.

a cubic symmetry (space group $I\bar{4}3d$, $a = 15.88552(5)$ Å) on heating at 570−600 K in vacuum better than 10^{-3} Pa.[21] This transformation was first detected inside electron microscopes and attributed to electron beam effects.[38] Our findings suggested that high vacuum inside electron microscopes ($\sim 10^{-6}$ Pa) and heating by the electron beam are responsible for the transformation. The crystal symmetry change from monoclinic to cubic is dramatic; however, the transformation occurs at rather soft conditions.[38] The $BiMnO_{3.03}$-to-$BiMnO_3$ transformation occurs at ambient pressure and mediate temperature. Therefore, a

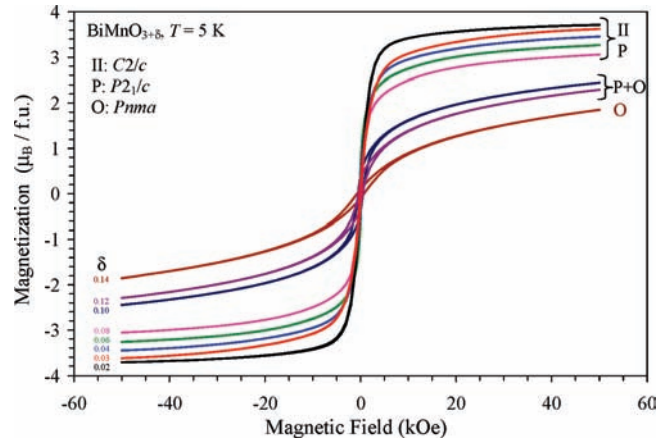

Figure 9. Isothermal magnetization curves at 5 K between −50 and 50 kOe for $BiMnO_{3+\delta}$ ($0.02 \le \delta \le 0.14$).

Table 3. Different Parameters Deduced from the Magnetization Curves of $BiMnO_{3+\delta}$[a]

δ	phase	μ_{eff} (μ_B)	μ_{cal} (μ_B)	θ (K)	T_C (K)	H_c (Oe)	M_r (μ_B)	M_S (μ_B)
0	I	4.93	4.90	123	102	3	0.013	3.92
0.02	II	5.07	4.86	118	84	85	0.160	3.72
0.03	II	5.01	4.84	119	82	135	0.208	3.63
0.04	II	4.97	4.83	119	80	220	0.412	3.46
0.06	P	4.90	4.79	113	71	210	0.631	3.27
0.08	P	5.08	4.75	99	68	185	0.371	3.06
0.10	P+O	4.98	4.71	93	60 (for P)	520	0.392	2.45
0.12	P+O	5.02	4.67	91	58 (for P)	490	0.292	2.29
0.14	O	4.85	4.64	88	27 (T_f)	720	0.100	1.85

[a] T_C is defined by the peak on the 100 Oe FC $d\chi T/dT$ vs T curve. μ_{eff} and θ are determined by the Curie−Weiss fit of the 10 kOe FC χ^{-1} vs T curves between 250 and 400 K. T_f is the spin-glass temperature. $\mathbf{H}_c$ is the coercive field, $\mathbf{M}_r$ is the remnant magnetization, and $\mathbf{M}_S$ is the magnetization at 5 K and 50 kOe. All the values are given per mole of $BiMnO_{3+\delta}$.

transformation from $BiMnO_3$ (with the $C2/c$ symmetry) to slightly-oxygen deficient $BiMnO_{3-\delta}$ (with possible symmetries of $C2$ or Cc) may also occur at very soft conditions because the $C2/c$ and $C2$ (Cc) structures are very close to each other. This idea can give a reasonable explanation for contradicting results in the literature. Thin-film samples of $BiMnO_3$ are usually grown under reduced oxygen pressure at high temperatures. Therefore, thin-film samples may be slightly oxygen deficient and have various symmetries. Observation of a long-range ordered structure with the $C2$ symmetry and a short-range ordered structure with the $P2$ or $P2_1$ symmetry in $BiMnO_3$ by selected-area electron diffraction can also be explained by the transformation inside electron miscroscopes.[18] However, we should note that oxygen-deficient $BiMnO_{3-\delta}$ samples cannot be prepared by direct high-pressure high-temperature synthesis,[21] similar to oxygen-deficient $LaMnO_{3-\delta}$ samples.[39] Careful reduction of $BiMnO_3$ and $LaMnO_3$ is necessary to produce oxygen-deficient samples.[39]

$BiMnO_{3.08}$ crystallizes in a monoclinic system but in the different space group of $P2_1/c$. The Mn2 site in $BiMnO_{3.08}$ has a strong Jahn−Teller distortion. Therefore, the Mn2 site should be occupied exclusively by Mn^{3+} ions. In other words, there should be no statistical distribution of Mn^{3+} and Mn^{4+} ions among the three sites. The Mn vacancies are localized mainly in one Mn1 site. These charge-ordering and vacancy-ordering

(38) Yang, H.; Chi, Z. H.; Li, F. Y.; Jin, C. Q.; Yu, R. C. *Phys. Rev. B* **2006**, *73*, 024114.

(39) Ruiz-Gonzalez, M. L.; Cortes-Gil, R.; Alonso, J. M.; Hernando, A.; Vallet-Regi, M.; Gonzalez-Calbet, J. M. *Chem. Mater.* **2006**, *18*, 5756.

scenarios are possible reasons for the crystal symmetry change in $Bi_{0.974}Mn_{0.974}O_3$ compared with $Bi_{0.99}Mn_{0.99}O_3$.

$BiMnO_{3.14}$ (a = 5.5136(4) Å, b = 7.8069(8) Å, and c = 5.5454(5) Å) has lattice parameters and structure similar to those of $LaMnO_{3+\delta}$ (for $LaMnO_3$-IIb,[22] a = 5.4954 Å, b = 7.7854 Å, and c = 5.5355 Å; for $LaMnO_{3.11}$,[23] a = 5.4963 Å, b = 7.7876 Å, and c = 5.5400 Å). The Mn−O bond lengths in $BiMnO_{3.14}$ (1.97 Å × 2, 1.98 Å × 2, and 2.00 Å × 2) are also close to those of $LaMnO_{3+\delta}$ (1.98 Å × 6).[22,23] However, no long-range magnetic ordering was found in $BiMnO_{3.14}$ compared with ferromagnetic $LaMnO_{3+\delta}$ ($LaMnO_3$-IIb[22] or $LaMnO_{3.11}$[23]). We note that very weak magnetic reflections were observed in orthorhombic $LaMnO_{3.15}$, and largely spin-glass behavior was suggested, similar to $BiMnO_{3.14}$.[40] In addition, further increase of the oxygen content in $BiMnO_{3+\delta}$ ($\delta \geq 0.16$) does not result in a rhombohedral phase, as in the case of $LaMnO_{3+\delta}$, but produces the $Bi_3Mn_3O_{11}$-type impurity.[33] The average oxidation state of Mn in $BiMnO_{3.14}$ is +3.28. This value is in good agreement with the BVS value of +3.27 calculated from the structural data. No short Bi−O bond lengths were found in $BiMnO_{3.14}$, and Bi^{3+} ions seem to behave similarly to La^{3+} ions, which do not have lone electron pairs.

There is one unusual feature in the magnetic properties of $BiMnO_{3+\delta}$ ($0.0 \leq \delta \leq 0.14$): the experimental effective magnetic moments (μ_{eff}) are almost the same in all the samples, independent of the amount of Mn^{4+}. In general, μ_{eff}'s are slightly larger in $BiMnO_{3+\delta}$ than in $BiMnO_3$. The reason for this is not clear right now. However, we should note that μ_{eff}'s were much larger than the calculated values for $LaMnO_{3+\delta}$.[24] There is decrease of the ferromagneitc transition temperature T_C with increasing δ for $0.0 \leq \delta \leq 0.10$, in comparison with the $LaMnO_{3+\delta}$ system, where an increase of T_C was observed for intermediate δ regions.[24,25] However, the decrease of T_C in $BiMnO_{3+\delta}$ is not monotonic. T_C drops by about 20 K on the transition from phase I ($\delta = 0$) to phase II ($\delta = 0.02$). T_C decreases a little in the stability range of phase II from 84 K for $\delta = 0.02$ to 80 K for $\delta = 0.04$. Then, T_C drops again by about 10 K on the crystal symmetry change from phase II to P-phase. T_C looks the same for the samples with $\delta = 0.10$ and 0.12, in agreement with their biphasic nature, where the samples consisted of the P- and O-phases with different fractions; the observed T_C corresponds to P-phases, which must have almost the same composition. $BiMnO_{3.14}$ demonstrates only spin-glass properties.[21] The Curie−Weiss temperature and saturated magnetization, $\mathbf{M}_S$, also decrease with increasing δ in $BiMnO_{3+\delta}$.

In conclusion, we have investigated the crystal and magnetic structures of $BiMnO_{3+\delta}$ as a function of the oxygen content. Ferromagnetic long-range magnetic ordering was found in $BiMnO_{3.03}$ and $BiMnO_{3.08}$. $BiMnO_{3.14}$ has no long-range ordering, despite the fact that it has the same crystal structure as ferromagnetic $LaMnO_{3.11}$. Charge-ordering and vacancy-ordering scenarios are suggested as possible reasons for the crystal symmetry change in $BiMnO_{3.08}$ compared with $BiMnO_{3.03}$. It was found that $BiMnO_{3.03}$ easily transforms to $BiMnO_3$ at rather soft conditions. Magnetic and chemical properties of $BiMnO_{3+\delta}$ ($0.02 \leq \delta \leq 0.14$) have also been investigated and compared with those of $LaMnO_{3+\delta}$. Systematic changes of magnetic parameters were found in $BiMnO_{3+\delta}$, depending on δ. Our work gives keystone results on the $BiMnO_{3+\delta}$ system.

Acknowledgment. This work was supported by World Premier International Research Center Initiative (WPI Initiative, MEXT, Japan) and by the NIMS Individual-Type Competitive Research Grant. This work was performed under the NIMS-RIKEN-JAEA Cooperative Research Program on Quantum Beam Science and Technology.

Supporting Information Available: Complete ref 6c; tables with bond lengths for all the samples; tables with the structural parameters for $BiMnO_{3.14}$ and $BiMnO_{3.03}$ (in the $C2$ and Cc models); specific heat data; details of XRD, DSC, and TGA results. This material is available free of charge via the Internet at http://pubs.acs.org.

JA102014N

(40) Hauback, B. C.; Fjellvag, H.; Sakai, N. *J. Solid State Chem.* **1996**, *124*, 43.